Infrastructure Assisted Constrained Connected Automated Vehicle Trajectory Optimization on Curved Roads: A Spatial Formulation on a Curvilinear Coordinate

Ran Yi[1], Yang Zhou[1], Xin Wang[2], Zhiyuan Liu[3], Xiaotian Li[1], Bin Ran[1]

[1]*Department of Civil and Environmental Engineering, University of Wisconsin-Madison, Madison, WI, USA*

[2]*Department of Industrial and Systems Engineering, University of Wisconsin-Madison, Madison, WI, USA*

[3]*Jiangsu Key Laboratory of Urban ITS, Jiangsu Province Collaborative Innovation Center of Modern Urban Traffic Technologies, School of Transportation, Southeast University, China*

Correspondence

Yang Zhou, Department of Civil and Environmental Engineering, University of Wisconsin-Madison, 1208 Engineering Hall, 1405 Engineering Drive, Madison, WI, 53706, USA

Email: zhou295@wisc.edu

Abstract: *Vehicle trajectory optimization is essential to ensure vehicles travel efficiently and safely. This paper presents an infrastructure assisted constrained connected automated vehicles (CAVs) trajectory optimization method on curved roads. This paper systematically formulates the problem based on a curvilinear coordinate which is flexible to model complex road geometries. Further, to deal with the spatial varying road obstacles, traffic regulations, and geometric characteristics, two-dimensional vehicle kinematics is given in a spatial formulation with exact road information provided by the infrastructure. Consequently, we applied a multi-objective model predictive control (MPC) approach to optimize the trajectories in a rolling horizon while satisfying the collision avoidances and vehicle kinematics constraints. To verify the efficiency of our method, a numerical simulation is conducted. As the results suggest, the proposed method can provide smooth vehicular trajectories, avoid road obstacles, and simultaneously follow traffic regulations, which is robust to road geometries and disturbances.*

1 INTRODUCTION

The CAVs equipped with advanced sensing and communication technologies enable their self-driving tasks and connection with other vehicles as well as infrastructures. Under such a connected and automated environment, CAVs can obtain precise ambient information via sensing and communication to make decisions and control more efficiently and safely than human-driven vehicles. Due to the potentials, CAV technologies have experienced a fast development in very recent years. Among these technologies, trajectory planning serves as a critical component to plan the vehicles' future movement to avoid hazards and make the CAVs operate in a safe, comfortable, and efficient manner.

Due to the importance, CAVs trajectory planning algorithms have been widely researched in recent years (e.g., Bohren et al., 2008; Gritschneder et al., 2018; Guo et al., 2018; Gutjahr et al., 2016; Manzinger et al., 2020; Mensing et al., 2011; Plessen, 2017; Werling et al., 2010, etc.). The state of art of CAV trajectory planning algorithms can be generally divided into four different approaches: (i) the graph search based approach (Bohren et al., 2008; Kala and Warwick, 2013); (ii) the interpolating curve planner (Fraichard and Scheuer, 2004; Labakhua et al., 2008; Reeds and Shepp, 1990) (iii) the sampling-based approach (Karaman et al., 2011; Kuwata et al., 2009); and (iv) the function optimization approach (Cremean et al., 2006; Kogan and Murray, 2006). The graph search based approach divides the feasible vehicle travel region into multiple grids, and by that, finding the optimal trajectory can be equivalently treated as finding the shortest path among nodes of feasible grids. By the shortest path formulation, this type of approach (Wu et al., 2020a; Wu et al., 2020b) usually applied dynamic programming and A-star algorithm. By the nature of the shortest path problem, this type of approach can be slow depending on the number of lattices and the resulting path may not continuous when the size of the grid is big. On the other hand, the interpolating curve planner, which uses predefined curve functions to generate reference points from the available space (e.g., Berglund et al., 2009; Labakhua et al., 2008; Pérez et al., 2013), is comparatively computational less expensive. The above-mentioned approaches largely ignore vehicle kinematics by assuming the physical positions are attainable regardless of vehicle speed and steering angle. The sampling-based approach executes a random search over the vehicle feasible state space (e.g., position, speed, acceleration) and finds an optimal sequence of state heuristically by comparing these randomly sampled state spaces according to a predefined objective function (e.g., minimize travel delay and intensive acceleration or brake, etc.). Though effective, these approaches usually render suboptimal solutions suggested by Elbanhawi and Simic (2014) due to the searching heuristics nature. As an opposite, the function optimization approach formulates the trajectory planning of CAV as a constrained optimization problem that is flexible in handling constraints from the environment (Gritschneder et al., 2018; Guo et al., 2018; Nolte et al., 2017), which can minimize a multi-objective cost function meanwhile satisfying the vehicle dynamics and hazard avoidances constraints. Further, the constrained optimization approach is usually implemented in a rolling horizon fashion to be against unexpected disturbances, and it is also known as MPC in the control theory field, which is widely applied in CAV car following control (Gong et al., 2016; Wang et al., 2019; Zheng et al., 2016).

Though promising, the constrained optimization based CAVs trajectory planning still faces some challenges. One challenge is to describe the road geometries in the formulation explicitly. Differed in the utilized coordinates, they can be further categorized as (i) CAV trajectory constrained optimization on a Cartesian coordinate (Gritschneder et al., 2018; Guo et al., 2018; Heilmeier et al., 2019; Nolte et al., 2017) and (ii) CAV trajectory constrained optimization on a curvilinear coordinate (Barfoot and Clark, 2004; Khalifa et al., 2019; Manzinger et al., 2020; Plessen, 2017). As a most widely applied coordinate, the Cartesian coordinate is more suited to describe open spaces. However, road geometry is usually composed of complex and composite curves, which means using Cartesian coordinates will be technically challenging to formulate the road boundaries as constraints. On the other hand, the curvilinear coordinate system is born to describe geometries formed by curved lines (Héry et al., 2017). Especially for the road geometry description, one axle of the curvilinear coordinate can be the lane centerline, while the other axle can be perpendicular to the centerline tangent. By that, the road geometry and boundaries can be simply formulated, reducing a great formulation and computation complexity.

Nevertheless, most of the vehicle trajectory optimization in the literature is vastly built by a temporal formulation (e.g., Guo et al., 2018; Gutjahr et al., 2016; Manzinger et al., 2020; Mensing et al., 2011; Plessen, 2017; Werling et al., 2010, etc.), assuming that the road geometry characteristics (e.g., curvature, lane tangent directions) remain unchanged over time, have not fully exploited the potentials of the curvilinear coordinate. The road geometries characteristics, traffic regulations (e.g., speed limit), and hazards are spatially varying rather than temporally varying, which serve as an un-observable exogenous disturbance impacting the performances further exert a negative impact on the desired planning objectives. Though the real-time information of road attributes can be conveyed to CAVs via V2I, with the increasing maturity of the vehicle to infrastructure (V2I) communication, explicitly incorporating these spatially varying characteristics in the temporal domain is still forbiddingly hard. However, the very recent works by Zhang et al. (2020) and Zhao et al. (2020), which utilize the spatial formulation for one-dimensional CAV car following control and Cartesian coordinate based human driven vehicles modeling in an intersection, respectively, provide a new angle to formulate the trajectory planning problems in a spatial domain. Inspired by their works, we found that the spatial domain formulation can explicitly incorporate the optimal formulation of spatially varying attributes on a curvilinear coordinate. Hence, an infrastructure assisted spatially constrained optimal CAV trajectory planning algorithm based on a curvilinear coordinate is provided in this paper. Especially, we contribute to design a spatially formulated constrained CAV trajectory optimization in a curvilinear coordinate which is capable of: (i) greatly simplifying the formulation compared with ones formulated in the time domain and Cartesian coordinates; (ii) quickly converges to the desired vehicle operation state (e.g., target speed, following lane centerline), and robust to the spatially disturbances (e.g., lane curvature change) by the infrastructure communication and assistance and (iii) providing a multi-objective optimization (e.g., smoothness of vehicle control, less deviation from desired state) framework which explicitly incorporates the spatial characteristics (e.g., lane curvature) and constraints (e.g., speed limit, obstacles, and lane width) while avoiding obstacles.

The organization of this paper is as follows. Section 2 provides detailed problem descriptions and gives assumptions of our paper. Section 3 describes the system by a state space and proves the controllability of our system. Section 4 presents the design of MPC for the system. Section 5 presents the results of the simulation experiments. Conclusion and future work are discussed in the final section.

2 PROBLEM DESCRIPTION

We provide an illustrative example to motivate our work on trajectory planning firstly. For our modeling, we only focus on the lane keeping processes without lane changing behaviors. When a CAV drives on a complex traffic scenario such as on a winding lane with or without a potential obstacle, as shown in Figure 1, an infinite number of paths are possible for a CAV, but limited time is given for the decision. It is assumed that one CAV can collect sensing data from not only its sensors but also road attributes (road geometry, traffic control devices) communicated with roadside units (RSUs) (Ran et al., 2020), by which CAVs know exact traffic environment information in advance. The purpose of the trajectory planning algorithm is to find the optimal path from an infinite number of possible paths based on the CAV's location in a very short time to ensure safety, control efficiency, comfort requirements, and traffic regulation obeyance. Before the detailed modeling, we made the following assumptions for the involved system.

Assumption 1: The vehicle is treated as a point.

Assumption 2: All actuation and communication delays are negligible.

Assumption 3: All vehicle dynamics effects such as suspension movement, road inclination, and aerodynamic forces are negligible.

Assumption 4: The road geometry characteristics, spatially traffic regulations and control (e.g., speed limit sign), and obstacle position information can be measured by RSU and communicate to CAVs.

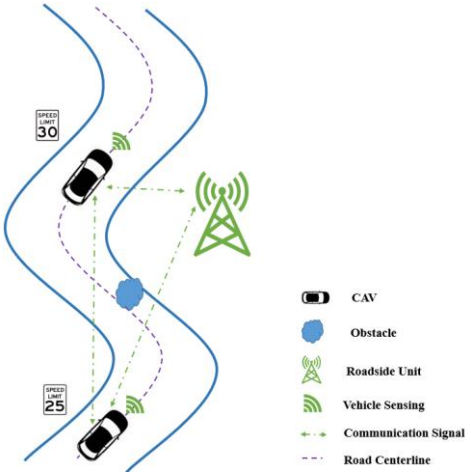

Figure 1 Problem Description.

3 STATE SPACE FORMULATION

In this section, we describe the system by a spatial domain state space in a curvilinear coordinate and prove its controllability. One axle of a curvilinear coordinate for a path is usually defined as its centerline, while the other axle can be perpendicular to the lane tangent. By that, road geometry and its boundaries can be simply formulated.

Let C represents the centerline of the lane as shown in Figure 2. The configuration of the centerline, with respect to the world-fixed inertial reference frame, $\{G\}$, is represented by the generalized coordinates $[x_{des}, y_{des}, \theta_{des}]^T \in R^3$, where its position is given by $[x_{des}, y_{des}]^T$ and its orientation in the global frame is represented by θ_{des}. Let s be the mapped length of the curvature along the lane centerline that vehicle has traveled. Based on that, we define $\{V\}$ represents the vehicle body-fixed reference frame with its speed $(v(s))$ represents the vehicle's forward direction and its orientation in the global frame is represented by $\theta_v(s)$.

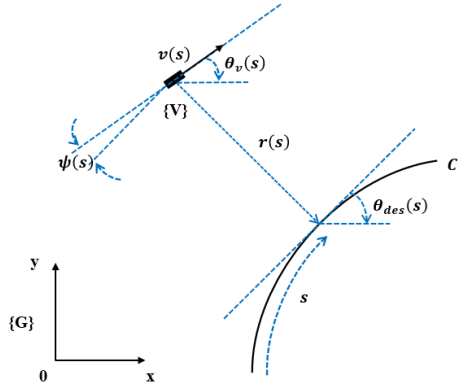

Figure 2 Vehicle Modelling on the Defined Curvilinear Coordinate.

To describe the vehicle dynamics over the established curvilinear coordinate, we construct a state space system and define the system state $X(s)$ for each space s as:

$$X(s) = \begin{bmatrix} r(s) \\ \psi(s) \\ p(s) \end{bmatrix}, \quad (1)$$

where $r(s)$ is the lateral deviation, which equals to signed orthogonal distance from the CAV to the closest point on the lane centerline C, in m; $\psi(s) = \theta_v(s) - \theta_{des}(s)$, where $\psi(s)$ is the angular deviation, θ_v is the angle between the CAV heading and the x-axis in the global frame {G} and $\theta_{des}(s)$ is the angle between the tangent of the lane centerline and the x-axis in the global frame {G}, in rad; $p(s) = p_v(s) - p_{des}(s)$, where $p(s)$ is the pace deviation, $p_v(s)$ is the reciprocal of the vehicular velocity and $p_{des}(s)$ is the reciprocal of the road speed limit ($p_{des}(s)$ is a nondifferentiable function of s, which can be treated as a constant), in s/m. Note that, $\theta_{des}(s)$ and $p_{des}(s)$ are spatially varying and got in a real-time manner by the infrastructure. Specifically, the vehicle dynamics are modeled as a nonlinear state space system as:

$$\frac{dX(s)}{ds} = \frac{d}{ds}\begin{bmatrix} r(s) \\ \psi(s) \\ p(s) \end{bmatrix} = \begin{bmatrix} \sin(\psi(s)) \\ k(s) \\ \alpha(s) \end{bmatrix} = f[X(s), U(s)], \quad (2)$$

where $k(s) = k_v(s) - k_{des}(s)$, which is the relative angular spatial change rate that can be seen as the control of the steering wheel. $k_v(s)$ is the curvature (reciprocal of vehicle turning radius) of the vehicle trajectory; $k_{des}(s)$ is the curvature of the lane centerline, in rad/m; and $\alpha(s)$ is relative moderation that indicates acceleration of the CAV, which can be treated as the control of the brake or throttle pedal (positive value indicates decelerating and negative value indicates accelerating), in s/m^2. $k(s)$ and $\alpha(s)$ compose our 'road characteristics compensated' control input $U(s)$, given as $U(s) = [k(s), \alpha(s)]^T$.

However, the road speed limit can be changed based on geometric road design in a real-world situation, which means $p_{des}(s)$ can not be treated as a spatially invariant constant when speed limit change occurs. Moreover, the speed limit change for the road is a unit jump and $p_{des}(s)$ is still a nondifferentiable function of s. To solve this problem, we introduce a "buffer zone" in front of the speed limit changing area where a changed speed limit is posted at the same length as our MPC model's prediction horizon. The "buffer zone" section divides speed limit difference by the "buffer zone" length to smoothly form a discrete velocity transit. With Δs is sufficiently small, the velocity change in the "buffer zone" is close enough to be treated as a continuous system. Thus $p_{des}(s)$ becomes a differentiable function of s inside the "buffer zone", and $\alpha_{des}(s)$ which is the parameter indicating acceleration of the road is the derivative of $p_{des}(s)$, in s/m^2. The new nonlinear function with the "buffer zone" introduced is $\frac{dX(s)}{ds} = \frac{d}{ds}\begin{bmatrix} r(s) \\ \psi(s) \\ p(s) \end{bmatrix} = \begin{bmatrix} \sin(\psi(s)) \\ k(s) \\ \alpha(s) \end{bmatrix}$, where $\alpha(s) = \alpha_v(s) - \alpha_{des}(s)$, where $\alpha_v(s)$ is the parameter indicating acceleration of the CAV, in s/m^2.

Given the state space defined above, we first analyzed its controllability which describes the ability of any control variables that can move the state of a system from any initial state to any final state in a finite time interval. Hence, we applied the following definitions and theorems to approve the controllability.

Theorem 1 Nonlinear system small-time locally controllability (Mahmoud, 2018)**:** The linear test: If a nonlinear $\dot{y} = f(y, u)$, whose linearized control system over an equilibrium point (y_e, u_e): $\dot{y} = Ay + Bu$ is controllable, then it is small-time locally controllable at (y_e, u_e).

Definition 1 Equilibrium point: For a nonlinear differential equation $\frac{dX(s)}{ds} = f[X(s), U(s)]$, where f is a function mapping $R^n \times R^m \to R^n$. A point $X_e \in R^n$ is called an equilibrium point if there is a specific $U_e \in R^m$ such that $f(X_e, U_e) = 0_n$.

By the **Definition 1**, it is trivial to find that the equilibrium point of the system as Eq. (2) occurs if and only if $X_e = [0,0,0]^T$, $U_e = [0,0]^T$

Theorem 2 Linear time-invariant system controllability (Mahmoud, 2018)**:** For a linear time-invariant system with the form $\dot{x} = Ax + Bu$, the controllability matrix can be written as:

$$G = G(A, B) = \underbrace{[B, AB, A^2B, \dots, A^{n-1}B]}_{n \times (mn)\ matrix}. \quad (3)$$

If $rank(G) = n$, this linear system is controllable.

Based on the **Definition 1, Theorem 1 and 2**, we can have the following Proposition:

Proposition: The state space formulated as Eq. (2) is small-time locally controllable at the equilibrium point $X_e = [0,0,0]^T$, $U_e = [0,0]^T$.

Proof:

With Taylor series, Eq. (2) at the equilibrium point (X_e, U_e) can be rewritten as:

$$\frac{dX(s)}{ds} = \sum_{i=1}^{n} \left[\frac{\frac{d^i f\left(X(s),U(s)\right)}{d^i X(s)}_{X(s)=X_e} (X(s)-X_e)^n}{n!} + \frac{\frac{d^i f\left(X(s),U(s)\right)}{d^i U(s)}_{U(s)=U_e} (U(s)-U_e)^n}{n!} \right]. \tag{4}$$

According to the Taylor series, a representation of a function as an infinite sum of terms that are calculated from the values of the function's derivatives at a single point. In our case, only 1st order derivative needs to be considered for the linearized control system. Moreover, the equilibrium in our system occurs when the CAV drives along the lane centerline, which means there is no deviation between the CAV and the lane centerline. The 1st order derivative of Eq. (4) at the equilibrium point (X_e, U_e) can be written as:

$$\frac{dX(s)}{ds} = \begin{bmatrix} 0 & \cos(\psi) & 0 \\ 0 & 0 & 0 \\ 0 & 0 & 0 \end{bmatrix}_{\psi=\psi_e} (X(s)-X_e) + \begin{bmatrix} 0 & 0 \\ 1 & 0 \\ 0 & 1 \end{bmatrix} (U(s)-U_e), \tag{5}$$

and Eq. (5) can be simplified as:

$$\frac{dX(s)}{ds} = AX(s) + BU(s), \tag{6}$$

where $A = \begin{bmatrix} 0 & 1 & 0 \\ 0 & 0 & 0 \\ 0 & 0 & 0 \end{bmatrix}$, $B = \begin{bmatrix} 0 & 0 \\ 1 & 0 \\ 0 & 1 \end{bmatrix}$.

Based on Eq. (3), the controllability matrix of Eq. (6) can be written as:

$$G(A,B) = [B, AB, A^2B] = \begin{bmatrix} 0 & 0 & 1 & 0 & 0 & 0 \\ 1 & 0 & 0 & 0 & 0 & 0 \\ 0 & 1 & 0 & 0 & 0 & 0 \end{bmatrix}, \tag{7}$$

which gives us the rank of the controllability matrix:

$$rank G(A,B) = rank \begin{bmatrix} 0 & 0 & 1 & 0 & 0 & 0 \\ 1 & 0 & 0 & 0 & 0 & 0 \\ 0 & 1 & 0 & 0 & 0 & 0 \end{bmatrix} = 3. \tag{8}$$

Remark 1

The above linearization process can also be proved by the small-angle approximation. Specifically, when the angle is relevant small and $\cos(\psi) \approx 1$, the small-angle approximation can be applied. The same state-space model, as Eq. (6), can be derived based on the small-angle approximation from Eq. (2).

We applied the zero[th]-order hold (ZOH) discretization technique for the control input to reflect the control frequency in the real-world application and facilitate the control formulation in the next section. Specifically, the control input is assumed constant during each update spatial interval Δs, and when Δs is sufficiently small, the discretization process is close enough to the continuous system (Chen et al., 2004). The discrete version of Eq. (5), according to Eq. (6), is shown as below:

$$X_{(m+1)\Delta s} \approx A_d X_{m\Delta s} + B_d U_{m\Delta s}, \forall m > 0 \tag{9-a}$$

$s.t.$

$$A_d = e^{A\Delta s}, \tag{9-b}$$

$$B_d = \int_0^{\Delta s} e^{A\gamma} d\gamma B. \tag{9-c}$$

For notation brevity, we use X_m to represent $X_{m\Delta s}$ for the rest of the paper.

4 MPC FORMULATION

In this section, we provide an MPC formulation due to its great capability to systematically deal with system state and control constraints and meanwhile handling multi-objectives. Further, it is robust to be against system disturbances due to its rolling horizon implementation. Based on the discretized control Eq. (9-a), a linear MPC formulation is considered in this study. In the proposed MPC framework as illustrated by Figure 3, at each current space step m, we solved a constrained trajectory optimization problem over a fixed finite prediction horizon with spatial length m_p to calculate the optimal control input and state sequences within the horizon. The controller only implements the first step optimal control input at space step m, and the algorithm continue this process repetitively until the end of algorithm, shown as Figure 3.

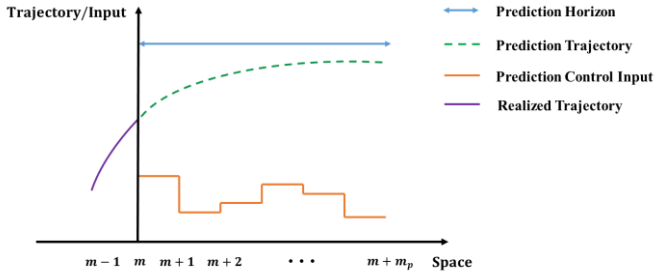

Figure 3 Illustration of Model Predictive Control.

To better illustrate the algorithm, we use $\mathcal{U}_m^p = \left[U_m^{p,m}, U_{m+1}^{p,m}, \dots, U_{m+m_p-1}^{p,m}\right]$ to denote the optimal control sequence for CAV obtained at space m for the prediction horizon, m to $m+m_p$; $\mathcal{X}_m^p = \left[X_m^{p,m}, X_{m+1}^{p,m}, \dots, X_{m+m_p}^{p,m}\right]$ to denote the predicted future states for CAV obtained at space m for the prediction space horizon, m to $m+m_p$; $\mathcal{X}_m^r = [X_0^r, X_1^r, \dots, X_m^r]$ to denote the realized states for CAV by space m, which can be seen as the optimal solution where X_0^r is the initial state when the control initiates.

By carefully considering the control efficiency and driving smoothness, we formulate an optimal control problem given as:

$$\left(\mathcal{X}_m^{p*}, \mathcal{U}_m^{p*}\right) = arg\ min\ F\left(X_{m+m_p}^{p,m}\right) + \sum_{i=m}^{m+m_p-1} L\left(X_i^{p,m}, U_i^{p,m}\right) \tag{10-a}$$

$s.t.$

$$X_{i+1}^{p,m} = A_d X_i^{p,m} + B_d U_i^{p,m} \forall i \in \{m, m+1, m+2, \dots, m+m_p-1\}, \quad (10\text{-b})$$

$$X_m^{p,m} = X_m^r, \quad (10\text{-c})$$

$$X_i^{p,m} \in \mathbb{X}_i \ \forall i \in \{m, m+1, m+2, \dots, m+m_p\}, \quad (10\text{-d})$$

$$U_i^{p,m} \in \mathbb{U}_i \ \forall i \in \{m, m+1, m+2, \dots, m+m_p\}, \quad (10\text{-e})$$

where m_p is the prediction space horizon; $L\left(X_i^{p,m}, U_i^{p,m}\right)$ is the running cost consists of the CAV penalties on the deviation from equilibrium point and driving discomfort; and $F\left(X_{m+m_p}^{p,m}\right)$ is the terminal cost that penalizes a deviation from the equilibrium point X_e at the final stage (i.e., the end of the prediction horizon). Eq. (10-c) is the initial condition constraint equal to the measured state at space step m; and Eq. (10-d) is the state constraint to regulate the transition vehicle states at each space point. The constraint in Eq. (10-e) is used to guarantee that the commanded steering wheel rotation and acceleration are within a reasonable range of $U(s)$.

For the objective function formulated in Eq. (10-a), we specify the running cost as follows:

$$L\left(X_{m+n}^{p,m}, U_{m+n}^{p,m}\right) = \left(X_{m+n}^{p,m}\right)^T P X_{m+n}^{p,m} + \left(U_{m+n}^{p,m}\right)^T Q U_{m+n}^{p,m} + 2q_1 k_{v,m+n} k_{des,m+n} - q_1 k_{des,m+n}^2, \quad (11\text{-a})$$

where P and Q are positive definite diagonal coefficients matrices, which are usually designed as the diagonal matrix below:

$$P = \begin{bmatrix} p_1 & & \\ & p_2 & \\ & & p_3 \end{bmatrix}, p_1, p_2, p_3 > 0, \quad (11\text{-b})$$

$$Q = \begin{bmatrix} q_1 & \\ & q_2 \end{bmatrix}, q_1, q_2 > 0. \quad (11\text{-c})$$

Especially, if we want to regulate that the vehicles stick to the lane centerline for safety concern, we can predefine p_1 and p_2 with large values, while on the other hand, if we are willing to provide the trajectories with flexibility, we can set $p_{1,2} \to 0$.

We further specify the terminal cost as:

$$F\left(X_{m+m_p}^{p,m}\right) = \left(X_{m+m_p}^{p,m}\right)^T S X_{m+m_p}^{p,m}, \quad (12)$$

where S is positive definite diagonal coefficients matric which is designed as $S = \begin{bmatrix} s_1 & & \\ & s_2 & \\ & & s_3 \end{bmatrix}, s_1, s_2, s_3 > 0.$

In Eq. (10-d) and (10-e), by considering collision-free constraints, steering wheel, and acceleration/deceleration limits, CAV's state constraint determined at space m is formulated in detail as:

$$r_{m+n}^L \le C X_{m+n}^{p,m} \le r_{m+n}^U \ \forall n \in \{0,1,2, \dots, m_p\}, \quad (13\text{-a})$$

$$\psi_{min} \le D X_{m+n}^{p,m} \le \psi_{max} \ \forall n \in \{0,1,2, \dots, m_p\}, \quad (13\text{-b})$$

$$0 \le T X_{m+n}^{p,m} \le +\infty \ \forall n \in \{0,1,2, \dots, m_p\}, \quad (13\text{-c})$$

$$-\frac{1}{R_{min}} - k_{des}(m+n) \le E U_{m+n}^{p,m} \le \frac{1}{R_{min}} - k_{des}(m+n) \ \forall n \in \{0,1,2, \dots, m_p-1\}, \quad (13\text{-d})$$

$$\alpha_{min} \le I U_{m+n}^{p,m} \le \alpha_{max} \ \forall n \in \{0,1,2, \dots, m_p-1\}. \quad (13\text{-e})$$

Eq. (13-a) is the constraint to make sure that the CAV drives within the drivable lane, where $C = [1,0,0]$, and $r_{m+n}^L = \begin{cases} r_{m+n}^-, \ if \ O_b \le m+n \le O_e \\ -r_{max}, \ Otherwise \end{cases}$ and $r_{m+n}^U = \begin{cases} r_{m+n}^+, \ if \ O_b \le m+n \le O_e \\ r_{max}, \ Otherwise \end{cases}$. Where r_{m+n}^- and r_{m+n}^+ are lower bound and upper bound that CAV can pass through within the obstacle zone, respectively; O_b and O_e are spatial positions where obstacle start and end; r_{max} is the half of the lane width; Eq. (13-b) is the constraint that the physical limits of allowable angular deviation for CAV, where $D = [0,1,0]$, ψ_{min} and ψ_{max} indicates the lower and upper bound of allowable angular deviation; Eq. (13-c) is the constraint to make sure that the CAV does not exceed the speed limit, where $T = [0,0,1]$; Eq. (13-d) is the constraint that the realized moving path of CAV is bounded by a given minimum turning radius, where $E = [1,0]$, R_{min} is the minimum turning radius of the CAV. Eq. (13-e) is the constraint that the realized acceleration/deceleration for CAV within the physical limits of α, where $I = [0,1]$, α_{min} is CAV's deceleration and α_{max} is CAV's acceleration limits.

To be noted that, the above formulation can be expanded in the scenario with speed limit change or stop sign by introducing the concept of "buffer zone", and correspondingly, Eq. (13-e) changes to $\alpha_{min} - \alpha_{des} \le I U_{m+n}^{p,m} \le \alpha_{max} - \alpha_{des} \ \forall n \in \{0,1,2, \dots, m_p-1\}$.

5 EXPERIMENT AND RESULTS

To test our optimal control model, we create a one-lane road segment with a series of curves as the numerical simulation environment shown in Figure 4. The road comprises three continuous curves with a total length of 1600 m and 3.6 m lane width which means a 1.8 m width from lane centerline to left/right lane boundary. The first two curves have the same radius of 300 m, and the radius of the third curve is 200 meters. The speed limit of the road is set as 54 km/h (15 m/s).

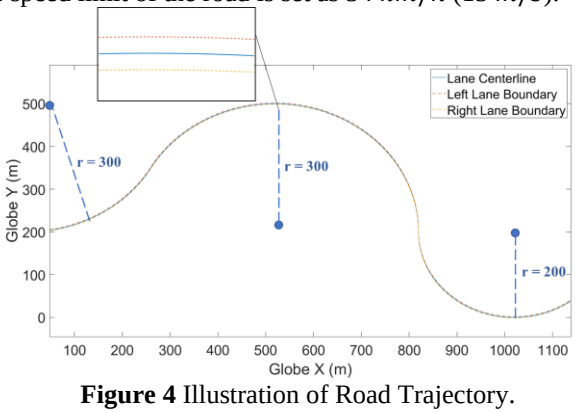

Figure 4 Illustration of Road Trajectory.

To validate our proposed method, a simulation experiment is performed on MATLAB since the field test is expensive and

beyond the scope of this paper. The parameter setting for the CAV trajectory optimization as Eqs. (10) is given in Table 1, according to Zhao et al. (2020) and Zhou et al. (2020).

Table 1 Default Parameters for Model Validation

Parameters	Value
$\boldsymbol{\psi_{min}}$ and $\boldsymbol{\psi_{max}}$	$-\pi/6\ rad$ and $\pi/6\ rad$
$\boldsymbol{a_{min}}$ and $\boldsymbol{a_{max}}$	-5 m/s^2 and 3 m/s^2
$\boldsymbol{r_{max}}$	1.8 m
$\boldsymbol{p_1}$, $\boldsymbol{p_2}$ and $\boldsymbol{p_3}$	0.33, 0.1 and 10
$\boldsymbol{q_1}$ and $\boldsymbol{q_2}$	1 and 500
$\boldsymbol{s_1}$, $\boldsymbol{s_2}$ and $\boldsymbol{s_3}$	$5p_1$, $5p_2$ and $5p_3$
$\boldsymbol{\Delta s}$	2 m
$\boldsymbol{m_p}$	80 m

5.1 Scenario 1: a continuous curvy road segment with the constant speed limit

For the initial condition, we set the vehicle's lateral deviation from the lane centerline to be 1 m, the angular deviation to be $-\frac{\pi}{6}\ rad$ and the pace deviation to be $\frac{1}{30}\ s/m$ (equivalently desired speed difference 5 m/s in our case). To better analyze the convergence behavior of the proposed algorithm, we plot the proposed controller performance of the first 50 m in Figure 5, which demonstrates the proposed trajectory optimization method's performance without the "buffer zone" introduced. To be noted that system states and control inputs maintain very closely to the system equilibrium point with nearly no oscillation from 50 m to 1600 m. Figure 5(a)-(c) and Figure 5(d)-(e) indicate the system state evolution, including lateral deviation, angular deviation, and pace deviation, and how the control inputs change in the space domain as the CAV moves by our control, respectively. As can be seen, similar trends are observed for different system states and the control input values. To be more specific, the lateral deviation exhibits some reasonable fluctuation initially: CAV moves 1.386 m laterally from lane centerline's left side to the right side in the first 6 m along the road, where the positive sign indicates that the CAV has been off the track and is at the left side of the lane centerline and the negative sign indicates that the CAV has off the track and is at the right side of the lane centerline. Then it quickly turns back from the right side to the lane centerline in the next 6 m and keeps driving on the lane centerline afterward. Angular deviation and relative angular spatial change rates converge in a nearly similar fashion as lateral deviation. As for the pace deviation and relative moderation converges to zero gradually. These results show that the algorithm quickly finds the difference between the vehicle states and the lane centerline and calculates the optimal control inputs to achieve the system equilibrium dynamically. Moreover, even though the $\theta_{des}(s)$ and $k_{des}(s)$ evolve spatially, the proposed controller shows great robustness to these disturbances mentioned above. Rather than the time-domain approach (e.g., Chen et al., 2014), the proposed method can better handle the space varying $\theta_{des}(s)$ and $k_{des}(s)$, which shows the superiority of proposed algorithm by incorporating the road geometric attributes via infrastructure to vehicle communication.

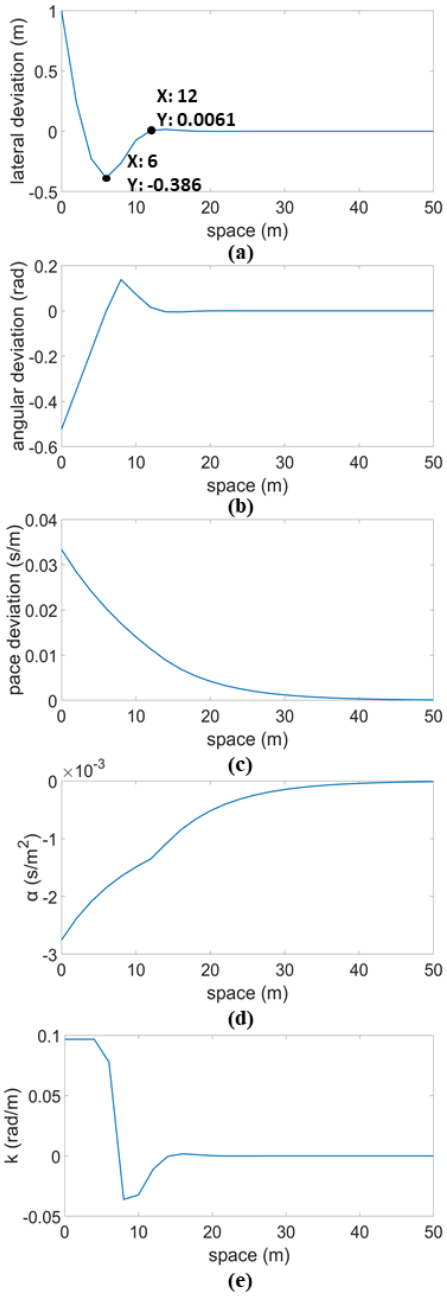

Figure 5 CAV State and Control Results of the first 50 Meters: (a) Lateral Deviation $r(s)$; (b) Angular Deviation $\psi(s)$; (c) Pace Deviation $p(s)$; (d) Relative Moderation $\alpha(s)$; (e) Relative Angular Spatial Change Rate $k(s)$.

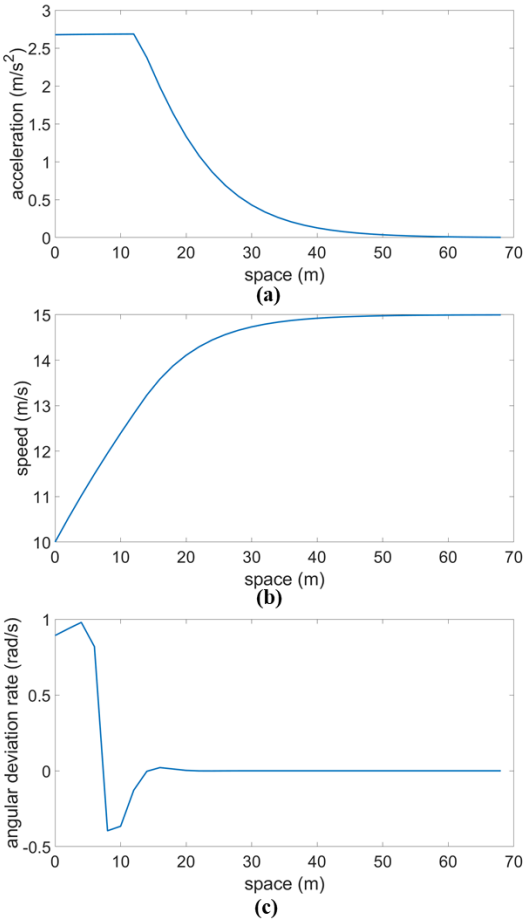

Figure 6 Speed, Acceleration and Angular Deviation Rate of CAV without the "buffer zone": (a) Acceleration; (b) Speed; (c) Angular Deviation Rate.

To gain further insight into the proposed trajectory optimization method, we convert $p_v(s)$, $\alpha(s)$ and $k_v(s)$ in the spatial domain into speed, acceleration, and angular deviation rate in the time domain, as shown in Figure 6. The CAV starts with and keeps a high acceleration for the first 15 m, and then it decreased gradually until it achieves equilibrium points, as shown in Figure 6(a). These acceleration changes lead to a speed increase in the first 50 m, and make the speed converge to the desired speed, as shown in Figure 6(b). We can also find that the angular deviation rate is within a reasonable range initially, and gradually converges to zero.

5.2 Scenario 2: a curved road with two different desired driving behaviors

The previous sections demonstrated the performance of our proposed trajectory optimization method. In this section, we further conduct a comparison to see the p_1 and p_2 weight impact on the obedience to the lane centerline. To see the flexibility of CAV's decision, we set an obedient driving behavior with p_1 and p_2 as the default case, and a flexible one with weights approaches to zero. To better visualize, we create a new one-lane 150 m curvy road with the same CAV initial conditions and adjust the reference line's weight. The blue dots line in Figure 7 shows the result with original weight and the red dots line shows the result of all q_1, q_2, s_1 and s_2 changed to 0 which means that there is no reference line to follow.

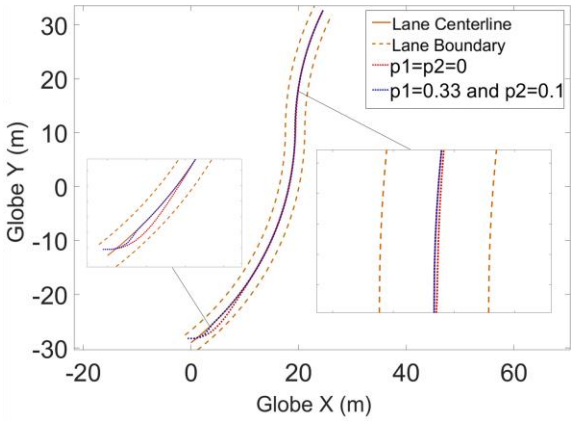

Figure 7 Comparison of Different p_1 and p_2 Values.

The results shown in Figure 7 illustrate that CAV makes much more aggressive decisions with the obedient driving behavior than those with the flexible driving behavior. As we can see, CAV with the obedient driving behavior makes sharp turning decisions and quickly turns back to the lane centerline. In contrast, CAV makes smooth turning decisions and needs more time to reach the lane centerline with the flexible driving behavior. Moreover, unlike CAV with obedient driving behavior tightly follows the reference line as long as it reaches the reference line, CAV with the flexible driving behavior can deviate from the reference line when the curve occurs.

5.3 Scenario 3: a curved road with an obstacle

We further conduct a simulation experiment using the same initial condition and one-lane road as shown in Figure 7 to test our proposed trajectory optimization method with a 10 m obstacle created. The $r_{m+n}^{L} = 0.5\ m$ and $r_{m+n}^{U} = 1.8\ m$ during the obstacle section. To meet both safety and driving comfort requirements, a joint driving mode is designed, which means a flexible driving behavior before and during the obstacle and an obedient driving behavior afterward.

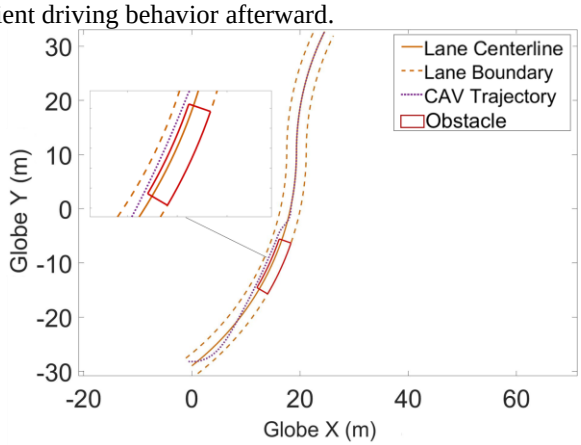

Figure 8 CAV Trajectory with Obstacle introduced.

As we can see from Figure 8, the CAV quickly detects the obstacle and makes smooth and comfortable control decisions to avoid the obstacle. The flexible driving behavior makes the CAV drive in the center to prevent any potential collision between the CAV and the obstacle during the obstacle section. In contrast, the obedient driving behavior lets the CAV quickly turn back and keep to the lane centerline after the CAV passes the obstacle section.

5.4 Scenario 4: a continuous curvy road segment with speed limit change

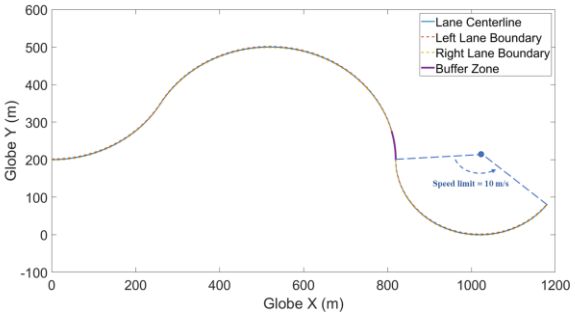

Figure 9 Illustration of Road Trajectory with a "buffer zone".

The results in the previous sections show that the proposed trajectory optimization method is efficient and stable without speed limit change to be considered. However, in order to test how the proposed trajectory optimization method works in a real-world situation, we change the speed limit of the road segment from 1104 m to 1600 m to be 10 m/s and create a "buffer zone" of the same length as m_p. In other words, we now pay our attention to a new situation where the road segment from 1024 m to 1104 m is replaced by the "buffer zone" with α_{des} equals $\frac{1}{1200}$ s/m^2. The illustration for the road trajectory with a "buffer zone" is given in Figure 9.

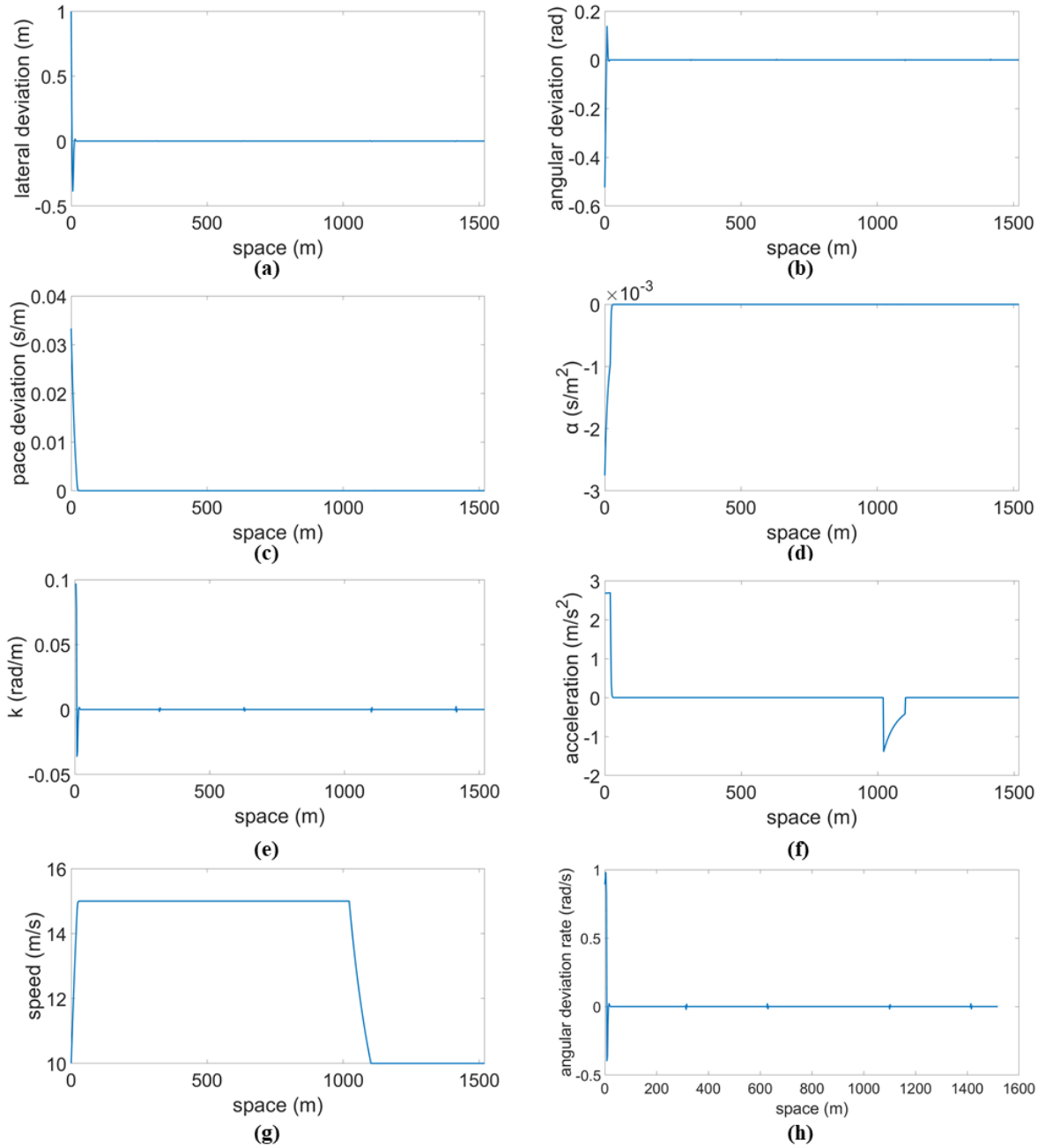

Figure 10 CAV State and Control Results with the "buffer zone": (a) Lateral Deviation $r(s)$; (b) Angular Deviation $\psi(s)$; (c) Pace Deviation $p(s)$; (d) Relative Moderation $\alpha(s)$; (e) Relative Angular Spatial Change Rate $k(s)$; (f) Acceleration; (g) Speed; (h) Angular Deviation Rate.

The results in Figure 10 give us a generalized illustration of how the proposed trajectory optimization method performs with the "buffer zone". Although the "buffer zone" is introduced, the system state evolution and how the control input change in the space domain, as shown in Figure 10(a)-(c) and Figure 10(d)-(e) respectively, is stable and show great robustness to the real-world disturbance. The change of angular deviation rate that indicates the relative turning speed and direction of the CAV shown in Figure 10(h) shows a similar trend as that in Figure 6(c). Furthermore, as expected, CAV's speed and acceleration oscillate around the "buffer zone".

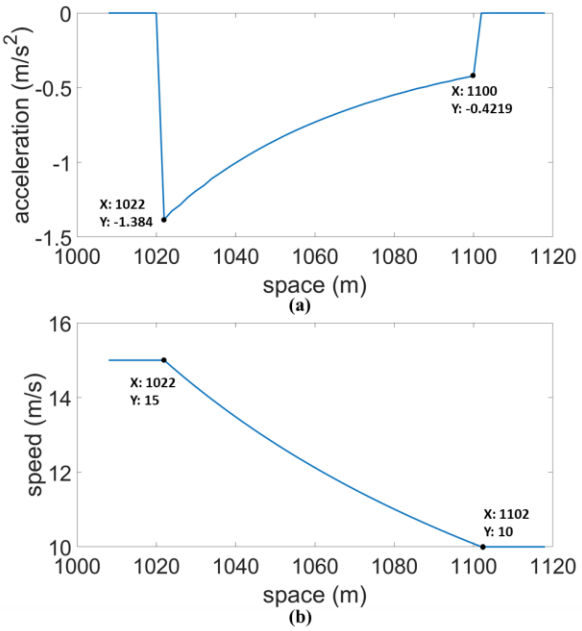

Figure 11 Speed and Acceleration inside the "buffer zone": (a) Acceleration; (b) Speed.

Figure 11 gives us a detailed illustration of CAV's speed and acceleration changes inside the "buffer zone". Figure 11(a) shows that the algorithm quickly detects the speed limit change in the "buffer zone" and makes the deceleration decision to achieve the system equilibrium dynamically, which leads to a smooth speed transition, as shown in Figure 11(b).

6 CONCLUSIONS

Vehicle trajectory optimization is essential to ensure vehicles travel efficiently and safely. Traditional trajectory planning algorithms and methods in time domain, by detecting the road information with a limited range and optimizing the trajectory myopically, which cannot well-handle the spatially varying road geometric change, obstacles, and traffic regulations. To remedy that, this paper provided a new angle to plan long-term trajectories in a spatial domain with the help of infrastructure. Specifically, this paper presented an infrastructure assisted spatially constrained optimal CAV trajectory planning algorithm based on a curvilinear coordinate. We systematically formulate the problem based on a curvilinear coordinate which is flexible to model complex road geometries. Further, to deal with the spatial varying road obstacles, traffic regulations, and geometric characteristics, two-dimensional vehicle kinematics is given state space in a spatial formulation with exact road information provided by the infrastructure. For rigor, the controllability of the state space was mathematically proved by using both the linear test and the small-angle approximation. Considering vehicle travel efficiency and trajectory smoothness while satisfying the collision avoidance and vehicle kinematics constraint, a multi-objective MPC was constructed, which can be efficiently solved by the state of arts optimization methods.

To demonstrate the usefulness and wide applications of our proposed trajectory planning optimization algorithm, multi-scenarios numerical simulations were conducted, which include four parts: (i) a continuous curvy road segment with the constant speed limit, (ii) a curved road with two different desired driving behaviors, (iii) a curved road with an obstacle, and (iv) a continuous curvy road segment with speed limit change. As the results suggested, the proposed trajectory optimization method could guarantee satisfactory performance for all scenarios under different types of disturbances. Further, the algorithm is capable of providing stable trajectory control with nearly no oscillation by utilizing the information provided by the infrastructure and newly presented formulation.

Nevertheless, some directions can be extended on the current framework in the future. For example, future studies could apply a more complex four-wheel vehicle control model and incorporate uncertainties in vehicle dynamics. Moreover, the MPC framework further considers the movement of ambient vehicles and plan CAVs' trajectories cooperatively.

ACKNOWLEDGEMENT

This research was supported by Wisconsin Traffic Operation and Safety (TOPS) Laboratory.

REFERENCE

Barfoot, T. D., & Clark, C. M. (2004). Motion planning for formations of mobile robots. *Robotics and Autonomous Systems*, *46*(2), 65–78.

Berglund, T., Brodnik, A., Jonsson, H., Staffanson, M., & Soderkvist, I. (2009). Planning smooth and obstacle-avoiding B-spline paths for autonomous mining vehicles. *IEEE Transactions on Automation Science and Engineering*, *7*(1), 167–172.

Bohren, J., Foote, T., Keller, J., Kushleyev, A., Lee, D., Stewart, A., … Satterfield, B. (2008). Little ben: The ben franklin racing team's entry in the 2007 DARPA urban challenge. *Journal of Field Robotics*, *25*(9), 598–614.

Chen, B. C., Luan, B. C., & Lee, K. (2014). Design of lane keeping system using adaptive model predictive control. *IEEE International Conference on Automation Science and Engineering (CASE)*, 922–926.

Chen, B. M., Lin, Z., & Shamash, Y. (2004). *Linear Systems Theory*. https://doi.org/10.1007/978-1-4612-2046-6

Cremean, L. B., Foote, T. B., Gillula, J. H., Hines, G. H., Kogan, D., Kriechbaum, K. L., … others. (2006). Alice: An information-rich autonomous vehicle for high-speed desert navigation. *Journal of Field Robotics*, *23*(9), 777–810.

Elbanhawi, M., & Simic, M. (2014). Sampling-based robot motion planning: A review. *Ieee Access*, *2*, 56–77.

Fraichard, T., & Scheuer, A. (2004). From Reeds and Shepp's to continuous-curvature paths. *IEEE Transactions on Robotics*, *20*(6), 1025–1035.

Frazzoli, E., Dahleh, M. A., & Feron, E. (2002). Real-time motion planning for agile autonomous vehicles. *Journal of Guidance, Control, and Dynamics*, *25*(1), 116–129.

Gong, S., Shen, J., & Du, L. (2016). Constrained optimization and distributed computation based car following control of a connected and autonomous vehicle platoon. *Transportation Research Part B: Methodological*, *94*, 314–334. https://doi.org/10.1016/j.trb.2016.09.016

Gritschneder, F., Graichen, K., & Dietmayer, K. (2018). Fast Trajectory Planning for Automated Vehicles using Gradient-based Nonlinear Model Predictive Control. *2018 IEEE/RSJ International Conference on Intelligent Robots and Systems (IROS)*, 7369–7374.

Guo, H., Shen, C., Zhang, H., Chen, H., & Jia, R. (2018). Simultaneous trajectory planning and tracking using an MPC method for cyber-physical systems: A case study of obstacle avoidance for an intelligent vehicle. *IEEE Transactions on Industrial Informatics*, *14*(9), 4273–4283.

Gutjahr, B., Gröll, L., & Werling, M. (2016). Lateral vehicle trajectory optimization using constrained linear time-varying MPC. *IEEE Transactions on Intelligent Transportation Systems*, *18*(6), 1586–1595.

Heilmeier, A., Wischnewski, A., Hermansdorfer, L., Betz, J., Lienkamp, M., & Lohmann, B. (2019). Minimum curvature trajectory planning and control for an autonomous race car. *Vehicle System Dynamics*, 1–31.

Héry, E., Masi, S., Xu, P., & Bonnifait, P. (2017). Map-based curvilinear coordinates for autonomous vehicles. *2017 IEEE 20th International Conference on Intelligent Transportation Systems (ITSC)*, 1–7.

Kala, R., & Warwick, K. (2013). Multi-level planning for semi-autonomous vehicles in traffic scenarios based on separation maximization. *Journal of Intelligent & Robotic Systems*, *72*(3–4), 559–590.

Karaman, S., Walter, M. R., Perez, A., Frazzoli, E., & Teller, S. (2011). Anytime motion planning using the RRT. *2011 IEEE International Conference on Robotics and Automation*, 1478–1483.

Khalifa, A., Kermorgant, O., Dominguez, S., & Martinet, P. (2019). An Observer-based Longitudinal Control of Car-like Vehicles Platoon Navigating in an Urban Environment. *2019 IEEE 58th Conference on Decision and Control (CDC)*, 5735–5741.

Kogan, D., & Murray, R. (2006). Optimization-based navigation for the DARPA Grand Challenge. *Conference on Decision and Control (CDC)*.

Kuwata, Y., Teo, J., Fiore, G., Karaman, S., Frazzoli, E., & How, J. P. (2009). Real-time motion planning with applications to autonomous urban driving. *IEEE Transactions on Control Systems Technology*, *17*(5), 1105–1118.

Labakhua, L., Nunes, U., Rodrigues, R., & Leite, F. S. (2008). Smooth trajectory planning for fully automated passengers vehicles: Spline and clothoid based methods and its simulation. In *Informatics in control automation and robotics* (pp. 169–182). Springer.

Mahmoud, M. S. (2018). *Advanced Control Design with Application to Electromechanical Systems*. Butterworth-Heinemann.

Manzinger, S., Pek, C., & Althoff, M. (2020). Using reachable sets for trajectory planning of automated vehicles. *IEEE Transactions on Intelligent Vehicles*.

Mensing, F., Trigui, R., & Bideaux, E. (2011). Vehicle trajectory optimization for application in ECO-driving. *2011 IEEE Vehicle Power and Propulsion Conference*, 1–6.

Nolte, M., Rose, M., Stolte, T., & Maurer, M. (2017). Model predictive control based trajectory generation for autonomous vehicles—an architectural approach. *2017 IEEE Intelligent Vehicles Symposium (IV)*, 798–805.

Pérez, J., Godoy, J., Villagrá, J., & Onieva, E. (2013). Trajectory generator for autonomous vehicles in urban environments. *2013 IEEE International Conference on Robotics and Automation*, 409–414.

Plessen, M. G. (2017). Trajectory planning of automated vehicles in tube-like road segments. *2017 IEEE 20th International Conference on Intelligent Transportation Systems (ITSC)*, 1–6.

Ran, B., Cheng, Y., Chen, T., Zhou, Y., Zhang, Z., Li, X., … Shi, K. (2020, July 30). *System and methods for partially instrumented connected automated vehicle highway systems*. Google Patents.

Reeds, J., & Shepp, L. (1990). Optimal paths for a car that goes both forwards and backwards. *Pacific Journal of Mathematics*, *145*(2), 367–393.

Wang, J., Gong, S., Peeta, S., & Lu, L. (2019). A real-time deployable model predictive control-based cooperative platooning approach for connected and autonomous vehicles. *Transportation Research Part B: Methodological*, *128*, 271–301.

Werling, M., Ziegler, J., Kammel, S., & Thrun, S. (2010). Optimal trajectory generation for dynamic street scenarios in a frenet frame. *2010 IEEE International Conference on Robotics and Automation*, 987–993.

Wu, J., Ah, S., Zhou, Y., Liu, P., & Qu, X. (2020). The Cooperative Sorting Strategy for Connected and Automated Vehicle Platoons. *ArXiv Preprint ArXiv:2003.06481*.

Wu, J., Kulcsár, B., Ahn, S., & Qu, X. (2020). Emergency vehicle lane pre-clearing: From microscopic cooperation to routing decision making. *Transportation Research Part B: Methodological*, *141*, 223–239.

Zhang, Y., Bai, Y., Wang, M., & Hu, J. (2020). Cooperative Adaptive Cruise Control With Robustness Against Communication Delay: An Approach in the Space Domain. *IEEE Transactions on Intelligent Transportation Systems*.

Zhao, J., Knoop, V. L., & Wang, M. (2020). Two-dimensional vehicular movement modelling at intersections based on optimal control. *Transportation Research Part B: Methodological*, *138*, 1–22. https://doi.org/10.1016/j.trb.2020.04.001

Zheng, Y., Li, S. E., Li, K., Borrelli, F., & Hedrick, J. K. (2016). Distributed model predictive control for heterogeneous vehicle platoons under unidirectional topologies. *IEEE Transactions on Control Systems Technology*, *25*(3), 899–910.

Zhou, Y., Ahn, S., Wang, M., & Hoogendoorn, S. (2020). Stabilizing mixed vehicular platoons with connected automated vehicles: An H-infinity approach. *Transportation Research Part B: Methodological*, *132*, 152–170.